Structure and electronic properties of ordered rare-earth (Ce,Dy)–transition-metal (Pd,Rh) surface compounds

W. Schneider
Institut für Oberflächenphysik und Mikrostrukturphysik, TU Dresden, 01062 Dresden, Germany

S. L. Molodtsov
Institut für Oberflächenphysik und Mikrostrukturphysik, TU Dresden, 01062 Dresden, Germany
and Institute of Physics, St. Petersburg State University, 198904 St. Petersburg, Russia

M. Richter
Max-Planck-Gesellschaft, Arbeitsgruppe Elektronensysteme, TU Dresden, 01062 Dresden, Germany

Th. Gantz, P. Engelmann, and C. Laubschat
Institut für Oberflächenphysik und Mikrostrukturphysik, TU Dresden, 01062 Dresden, Germany
(Received 6 October 1997)

Ordered rare-earth (RE)–transition-metal (TM) surface compounds have been prepared by thermal deposition of thin Ce and Dy films onto Rh(111) and Pd(111) substrates and subsequent annealing. Low-energy electron diffraction and Auger data suggest a crystallographic structure and stoichiometry isomorph to the (111) surface of the $AuCu_3$-type compound $(RE)(TM)_3$. Valence-band angle-resolved photoemission data of the films are in good agreement with optimized LDA-LCAO band-structure calculations of the corresponding $(RE)(TM)_3$ compounds. Particularly, an observed energy shift of the Pd $4d$-derived states to higher binding energies in the Ce-Pd system as compared to the Dy-Pd compound is correctly reproduced by the theory and related to a noninteger occupation of the Ce $4f$ states. [S0163-1829(98)00523-2]

I. INTRODUCTION

The recent discovery of superconductivity in rare-earth-Ni– and rare-earth-Pd–boron carbides with transition temperatures up to 25 K (Refs. 1–3) has renewed the interest in rare-earth (RE)–transition-metal (TM) compounds. A number of these compounds reveals interesting magnetic properties as well as other electron-correlation effects like mixed-valence or heavy-fermion behavior, which are caused by interactions of the open RE $4f$ shell with the partly occupied valence bands of the TM.[4]

RE-Pd compounds frequently behave differently from other RE-TM systems, due to the Pd $4d$-derived bands that become occupied in the compounds leaving the Fermi energy E_F in a region of low density of states (DOS). Due to this low DOS at E_F the magnetic coupling between localized $4f$ moments via the Ruderman-Kittel-Kasuya-Yosida mechanism becomes weak, and since the occupied Pd $4d$-derived states do not essentially contribute to magnetism, magnetic order is absent in RE-Pd systems or appears only at very low temperatures.[5] By the same way hybridization effects, that play a dominant role in Ce-TM systems,[6,7] become strongly reduced in Ce-Pd compounds.[8] Even the compound with the largest Pd concentration, $CePd_3$, represents only a moderately hybridized mixed-valent system,[9,10] while the Ce $4f$-states in the isostructural Rh compound are on the border of bandlike behavior.[9,11]

Investigations of the electron structure of RE-TM compounds by means of electron spectroscopies have mostly been concentrated on the properties of the $4f$ states. Studies on the valence bands were usually restricted to measurements of the density of states, since most of the experiments were performed on polycrystalline samples. Single-crystalline samples, necessary for angle-resolved mapping of electron bands, are difficult to obtain. Moreover, the preparation of clean, single-crystalline surfaces is not easy due to the high chemical reactivity of the RE's. As an alternative approach, experiments can be performed on ordered surface compounds, which are prepared *in situ* by deposition of RE's onto single-crystalline TM substrates followed by thermally driven surface or interface reactions. Of course, not all bulk phases can be prepared in this way. On the other hand, surface compounds, which differ in structure and stoichiometry from the existing bulk phases, may also be stabilized. Nevertheless, the resulting compounds reflect material properties potentially relevant for technological applications of these systems in form of thin films and multilayers.

In the present publication we report on angle-resolved photoemission (ARPE) studies of RE(Ce,Dy)-TM(Pd,Rh) surface compounds. The samples were prepared by *in situ* deposition of the RE elements onto clean Pd(111) and Rh(111) surfaces, followed by annealing of the interfaces at 1100 K. Low-energy electron diffraction (LEED) and Auger analyses of the films reveal a structure and chemical composition corresponding to the (111) surface of the cubic $AuCu_3$-type compounds $(RE)(TM)_3$. The ARPE data are in good agreement with band-structure calculations for these compounds. Particularly for $CePd_3$, an observed shift of the Pd $4d$-derived bands to higher binding energies as compared to their position in $DyPd_3$ is correctly reproduced by the theory and attributed to a noninteger occupation of the Ce $4f$ states.

II. EXPERIMENTAL DETAILS AND BAND-STRUCTURE CALCULATIONS

The ARPE experiments were performed at the Berliner Elektronenspeicherring für Synchrotronstrahlung (BESSY) exploiting synchrotron radiation from the toroidal-grating monochromator TGM1. Valence-band ARPE spectra were taken using a rotatable hemispherical electron-energy analyzer (VSW-ARIES) tuned to an energy resolution of about 150 meV (FWHM) and an angle resolution of 1°. All experiments were performed at a photon incidence angle of 30° relative to the sample surface.

Single-crystalline Pd(111) and Rh(111) substrates (1.5-mm-thick disks with diameters of 5–6 mm from MaTeck, Inc.) were cleaned by argon ion bombardment followed by a series of 10-min cycles of annealing at a temperature of 1100 K in an oxygen atmosphere of 5×10^{-8} mbar. The annealing was repeated until no carbon or other bulk-originating contaminations were detected by LEED and Auger-electron spectroscopy (AES). In order to desorb the oxidized surface layer the substrates were flashed during 10 sec at a temperature of 1400 K until characteristic sharp hexagonal LEED patterns and no oxygen contaminations in ARPE and AES spectra were observed. Dy and Ce were thermally evaporated at a rate of 3 Å/min from metal pieces inserted into W-Re coils. The evaporation rates as well as the thicknesses of the deposited layers were monitored with a quartz microbalance. During the experiments, the vacuum was better than 1×10^{-10} mbar. It shortly rose to 1×10^{-9} mbar during evaporation.

A deposition of 20–40 Å of RE's onto substrates kept at room temperature or at the temperature of liquid nitrogen resulted in nonordered overlayers. A following step-by-step annealing of the interfaces at increasing temperatures in the range from 1000 K to 1200 K led to sharp hexagonal (2×2) overstructures in the LEED patterns. Surface contaminations were checked by ARPE and AES and found to be negligible.

For the Dy-Pd system a simple quantitative analysis of the AES data gives an atomic concentration ratio of Dy to Pd close to 1/3. The observed (2×2) overstructure of the LEED pattern agrees with a crystalline structure isomorph to the (111) surface of the cubic $AuCu_3$-type phase $(RE)(TM)_3$.[12] Here, every second TM atom in every second row of each layer is replaced by a RE atom. This leads to a lattice mismatch less than 5% relative to the pure Pd(111) surface layer. The formation of these compounds upon annealing may, therefore, be considered as a simple replacement of Pd by RE's atoms leaving the Pd matrix almost unchanged. Identical LEED patterns could also be obtained from metallic films grown by codeposition of Dy and Pd in the atomic ratio 1 to 3 onto a W(110) substrate.[13] This observation gives further support for the formation of $(RE)(TM)_3$ compounds in the present case.

Band-structure calculations for the intermetallic compounds as well as for pure Pd and Rh metal were performed in the framework of the local-density approximation (LDA) with the standard Hedin-Lundquist exchange-correlation potential[14] exploiting the optimized method of linear combination of atomic orbitals[15] (LCAO) in its scalar relativistic version.[16] The used basis includes $5s$, $5p$, and $4d$ states for Pd and Rh; $6s$, $6p$, and $5d$ states for Dy; and $6s$, $6p$, $5d$, and $4f$ states for Ce. The treatment of the Dy $4f$ states as partially filled atomiclike core shell accounts for the localized behavior of these states in heavy RE's. The Dy $4f$ occupation was chosen to be 9, corresponding to a trivalent configuration. In contrast to the case of Dy-derived compounds, the $4f$ states in Ce-Pd and Ce-Rh systems were considered to be itinerant. The assumption of a normal metallic state with noninteger $4f$ occupation should yield an approximately correct ground-state charge distribution even if this ground state is mixed valent ($CePd_3$).[17] Using the linear tetrahedron method, the k sums were performed over a mesh containing 165 k points in the irreducible part of the Brillouin zone (BZ). The intermetallic compounds were handled as ideal crystals without accounting for surface and real structure effects.

Good agreement both with experimental data and with previous calculations was obtained for the weakly correlated $4d$ bands of Pd and Rh metal.[18–20] For the compounds, the results are in accordance with previous calculations[11,21,22] as well as with angle integrated photoemission[9,22] (PE) and inverse PE data[23,24] on several $(RE)(TM)_3$ compounds.

III. RESULTS

The valence-band structure of the grown surface compounds was studied by ARPE in a photon-energy range from 21.2 eV to 95 eV. Due to stoichiometry and cross-section effects, the valence-band spectra taken at these photon energies are dominated by emissions from TM $4d$ states. ARPE spectra from Ce/Pd(111) (2×2) taken at various photon energies in normal-emission geometry are shown in Fig. 1(a). The data have been normalized to equal maximum intensity. For the Ce-Pd system, the spectra are dominated by four features at approximately 1.2 eV, 2 eV, 3 eV, and 4.5 eV binding energy (BE). These features reveal intensity modulations but almost no dispersion upon variations of the photon energy. A steplike PE signal at the Fermi energy decreases when going from lower toward higher photon energies demonstrating a metallic character of the interface with predominantly sp-like states at E_F.

In Fig. 1(b), the observed peak positions were assigned to band-structure calculations for $CePd_3$. Free-electron-like final states and direct interband transitions in the reduced BZ scheme were assumed. The minimum of the parabolic energy-dispersion curve of the free-electron-like final states was pinned at the calculated bottom of the valence band. The parabolic slope was fitted to the corresponding s-like branch in the region close to the Γ-point by a proper choice of the effective electron mass. This standard approach that neglects the influence of the actual atomic potentials has been applied quite successfully to many solids. Particularly in the present case of a simple cubic symmetry and final states, which are energetically far above the unoccupied RE $4f$ states and RE $5d$-derived bands, this approach is expected to represent a satisfactory approximation of the real final states. Figure 1(b) reveals a reasonable agreement between band-structure calculations and PE data. However, the experimentally obtained dispersion of valence bands is somewhat weaker than what is predicted by the theory. This may point to a loss of translation symmetry in the direction perpendicular to the surface caused, for example, by (i) a quasi-two-dimensional nature

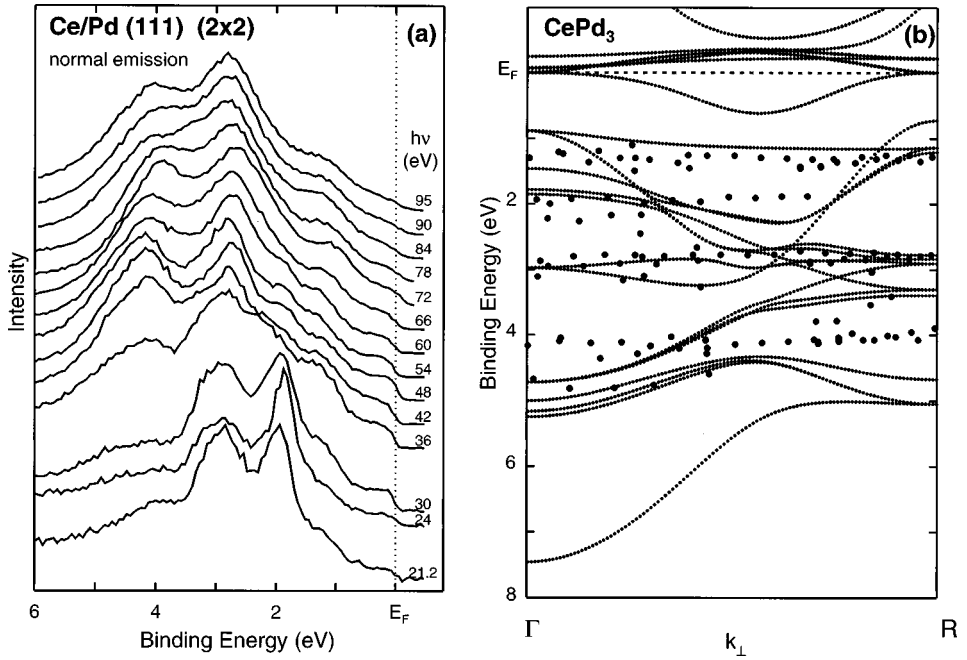

FIG. 1. (a) ARPE spectra of Ce/Pd(111) (2×2) taken at various photon energies in normal-emission geometry. (b) Assignment of the experimentally observed peak positions (solid circles) to calculated bands of $CePd_3$ (see text).

of the film or by (ii) a distorted stacking sequence of the crystallographic planes. Since the AES data indicate a film thickness, which is large as compared to the electron mean free path in the ARPE experiments (about 10 Å), possibility (i) may be ruled out. Respective spectra of an ordered Dy-Pd surface compound reveal similar dispersive behavior. Although, they differ from Ce-Pd data by an almost rigid energy shift to lower BE's of the Pd $4d$-derived bands. A similar phenomenon has been reported previously for a comparison of angle-integrated PE spectra of $CePd_3$ and $LaPd_3$ and has been related to the mixed-valent character of Ce.[9] As for Ce-Pd, the experimental results for Dy-Pd are in a reasonable agreement with band-structure calculations for the corresponding intermetallic compound with $(RE)(TM)_3$ composition.

In contrast to the normal-emission data, ARPE spectra taken at fixed photon energies and different emission angles reveal stronger dispersions of the valence-band features. Figure 2 shows ARPE spectra from (a) Dy/Pd (2×2) and (b) Ce/Pd (2×2) recorded at 33 eV photon energy along the $\bar{\Gamma}$-$\bar{K}$ direction of the surface BZ. In both compounds, the ARPE spectra taken at small polar angles Θ are character-

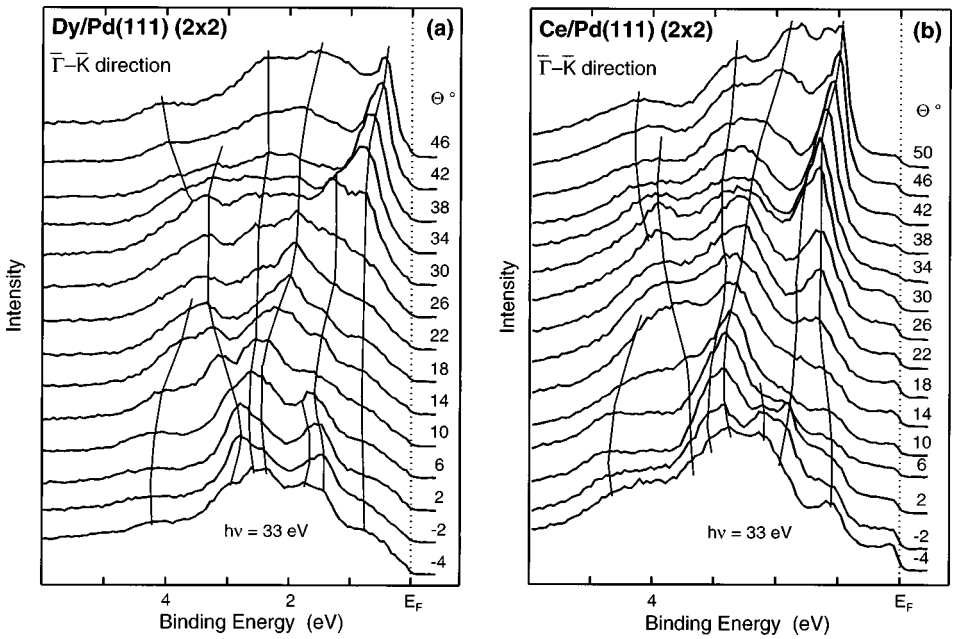

FIG. 2. ARPE spectra taken at $h\nu=33$ eV and various polar angles Θ for (a) Dy/Pd(111) (2×2) and (b) Ce/Pd(111) (2×2). Solid lines serve as guides to the eye marking dispersion of main emission features.

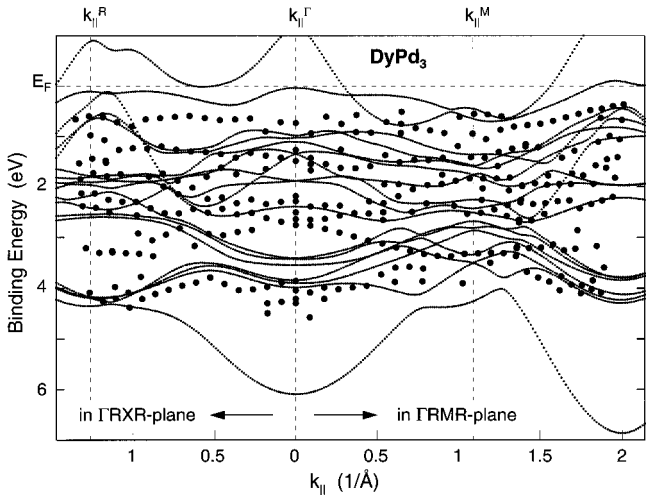

FIG. 3. Comparison of peak positions (solid circles) in ARPE spectra taken at $h\nu=33$ eV and various polar angles from Dy/Pd(111) (2×2) with calculated bands of $DyPd_3$ (see text).

ized by four main features. Two of them are split into substructures. Solid lines connecting corresponding peaks of different spectra serve as guides to the eye indicating the assumed dispersions. For the Dy-Pd system, the corresponding structures are shifted by about 0.6 eV toward lower BE's as compared to those for the Ce-Pd compound.

The dispersion of the ARPE structures is similar for both compounds. Upon angle variation from 0° to 18° in the Dy-Pd system, the 4.2-eV feature shifts to lower BE while one branch emerging from the 2.5-eV structure moves in the opposite direction. At $18°\leqslant\Theta\leqslant26°$ these two branches cross each other, giving rise to hybridization phenomena as shown by the band-structure calculations. Another two branches of the 2.5-eV feature, which are almost degenerated in ARPE spectra taken close to the normal-emission geometry, split up at larger emission angles. The 1.5-eV structure can clearly be identified only at small polar angles; it disappears at $\Theta>10°$. The lowest-lying feature recorded at about 0.8 eV BE at normal emission reveals almost no dispersion up to $\Theta\cong30°$. Then it moves slightly toward the Fermi energy, where its intensity strongly increases.

An assignment of the observed peak positions for Dy/Pd [see Fig. 2(a)] to the calculated bands of $DyPd_3$ is shown in Fig. 3. As before [Fig. 1(b)], we consider direct transitions into free-electron-like final states and assume conservation of the component of the electron momentum parallel to the surface, $k_{\parallel}$. The horizontal axis in Fig. 3 scales $k_{\parallel}$ values along the two high-symmetry directions in the BZ of the simple-cubic structure ($\Gamma-R$ and $\Gamma-M$) projected onto the (111) surface. The electron structure was calculated within the ΓRXR and ΓRMR planes in the extended BZ along a circle of constant energy corresponding to the mean energy of excited ($h\nu=33$ eV) electrons relative to the bottom of the valence band.[25] ARPE spectra of Ce/Rh(111) (2×2) taken at 33 eV photon energy and different emission angles are shown in Fig. 4(a). While in this figure the PE structures are less pronounced as compared to those of the RE-Pd systems, the observed dispersion of the valence bands is similar to the results obtained for Ce-Pd and Dy-Pd. The main difference to Ce-Pd, however, is a strong low-BE shift of the bands in Ce-Rh. This energy shift is even larger as compared to that obtained by the substitution of Ce by Dy in Pd-based compounds. It ranges to more than 1.0 eV for the low-BE PE features. The structure, observed at approximately 3 eV in the normal-emission spectra of Ce-Pd [Fig. 2(b)], appears now at about 2.5 eV in the corresponding electron energy distribution curves of the Ce-Rh surface compound. The most pronounced sharp feature, which is seen for $\Theta>22°$ at

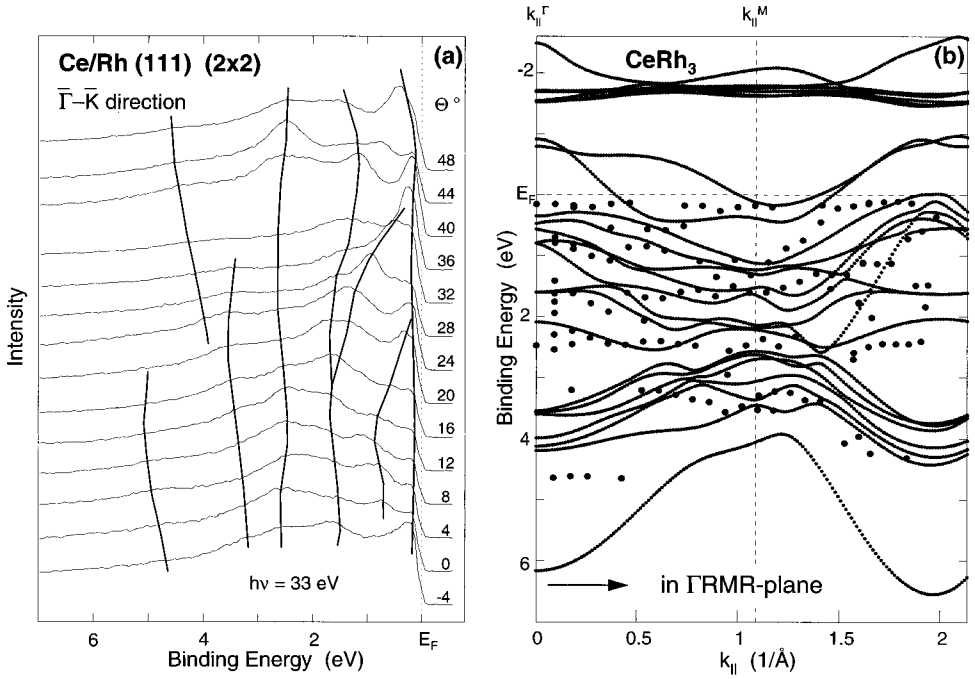

FIG. 4. (a) ARPE spectra taken at $h\nu=33$ eV and various polar angles Θ for Ce/Rh(111) (2×2). (b) Assignment of the experimental data (solid circles) to calculated bands of $CeRh_3$ (see text).

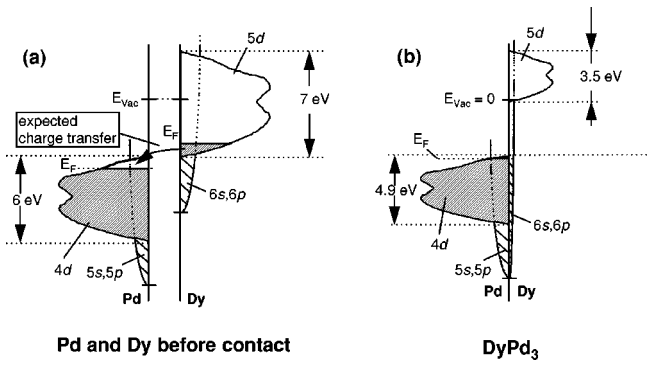

FIG. 5. Tight-binding model illustrating the formation of the pseudogap due to charge transfer and band narrowing (see text).

1.0–1.2 eV BE in Ce-Pd, is shifted directly to E_F in the Ce-Rh system.

Figure 4(b) shows a comparison of the energy positions of the experimentally observed peaks for the Ce-Rh system and results of band-structure calculations for $CeRh_3$. In analogy to the analysis performed for Dy-Pd (Fig. 3) the ARPE data were assigned to electron bands calculated within the ΓRMR plane along a circle of the corresponding constant energy. The calculated bands are projected onto a plane parallel to the sample surface. In agreement with the experiment the calculated band dispersion remains qualitatively the same upon substitution of Pd by Rh. The energy positions of different branches, however, are shifted toward the Fermi energy in the Rh-based compound. This shift is larger for low-BE branches. It becomes insignificant at the bottom of the valence band. As in the case of the Pd-based compounds a good agreement between ARPE results taken from the Ce/Rh(111) (2×2) interface and calculated bands of the $CeRh_3$ compound is obtained.

To our knowledge, $DyRh_3$ does not exist as a bulk phase.[26] Notwithstanding, LEED patterns obtained for the Dy-Rh system are identical to the patterns observed for the $CeRh_3$ compound. Furthermore, the experimentally observed valence-band ARPE structure of Dy/Rh(111) (2×2) is in good agreement with the calculated bands of a hypothetic $AuCu_3$-type compound $DyRh_3$ and very similar to the Ce-Rh data shown in Fig. 4(a). Thus, one may conclude, that this phase could be stabilized in thin films.

IV. DISCUSSION

As a first approach to a better understanding of the electron structure of the $(RE)(TM)_3$ phases a simple model may be considered that describes compound formation in terms of charge transfer between microscopic pieces of RE's and TM's.[27] Charge transfer is governed by the electron densities and the contact potential, which are related to the individual densities of states and work functions, respectively. The partial sp and d DOS of pure Dy and Pd metals are sketched in the left pannel of Fig. 5, plotted with respect to a common energy zero E_{vac}. With about nine d electrons per atom, the Pd $4d$ band is almost filled, while for the RE metal the $5d$-band occupation is close to 1, and the Fermi energy lies close to the bottom of this band. When bringing these metals into contact, the contact potential leads to a charge transfer from the RE to Pd until a common Fermi energy is established. Since in a PE experiment binding energies are measured relative to the Fermi energy, this charge transfer is reflected in the ARPE spectra by a shift of the Pd $4d$ band to higher BE. Upon compound formation, in addition to the charge transfer band narrowing occurs due to the reduced coordination with equivalent atoms. Within a simple tight-binding formalism, this band narrowing is proportional to the square-root of the coordination number N.[28] In the present case of Pd, N reduces from 12 in the metal to 8 in the $(RE)Pd_3$ compounds resulting in a contraction of the $4d$ band by a factor of 0.8. For the RE's, this effect is more dramatic, since in the compounds the RE atoms are surrounded only by Pd neighbors. The RE neighbors appear first in the second coordination shell. Assuming that the RE atoms in the second shell contribute to the bandwidth only half as much as nearest neigbors, the effective coordination of the RE atoms reduces from 12 in the pure metal to 3 in the compounds causing a narrowing of the RE $5d$ band by a factor of 0.5. Due to the band contraction a broad pseudogap between Pd $4d$- and RE $5d$-derived states is formed. Since within this simple model only about one $5d$ electron is transferred to three Pd atoms, the charge transfer is too small to fill the Pd $4d$ bands completely. Therefore, the Fermi energy becomes stabilized close to the top of the Pd $4d$-derived valence band.

A more elaborate discussion should take into account the hybridization between RE $5d$ and TM d states that gives rise to RE $5d$ contributions to the occupied TM d band and TM d contributions to the unoccupied part of the RE $5d$ band. This kind of hybridization is particularly essential for the understanding of the magnetic coupling between $3d$ and $5d$ states in TM-rich hard magnetic RE-TM compounds.[29] In this sence, one could also speak in terms of a covalency gap separating occupied and unoccupied d states: Anyhow, already the simplified picture is in good agreement with PE and Bremsstrahlung-isochromat-spectroscopy (BIS) experiments on several $(RE)Pd_3$ compounds.[9,23]

The effect of valency of the RE's can also be visualized within this simple model. Treating the $4f$ states as narrow bands pinned at the Fermi energy, a larger charge transfer to Pd becomes possible leading to a filling of the Pd $4d$-derived bands and to stabilization of the Fermi level in the pseudogap between Pd $4d$- and RE $5d$-derived states due to the partially occupied $4f$ states. This pinning of the Fermi-level position is reflected in the ARPE experiments by an almost rigid shift to higher BE of the valence-band emissions in $CePd_3$ as compared to those in $DyPd_3$. Replacing Pd by Rh, the $4d$ occupation is reduced, and even the additional charge supplemented from the $4f$ states of Ce is not sufficient to fill the $4d$ band. Consequently, the Fermi energy remains pinned near the top of the valence band almost independent of the $4f$ occupation. The Ce $4f$ band is still located within the $4d$-$5d$ gap, that now is formed well above the Fermi level. This scenario is in accordance with experimental results of the present work, where only small differences have been observed between the valence-band ARPE spectra of $DyRh_3$ and $CeRh_3$. The above model is also in agreement with previous BIS experiments, where the position of the Ce $4f^1$ final state was found to be shifted from 0.5 eV to 1.6 eV above the Fermi energy when going from $CePd_3$ to $CeRh_3$.[24]

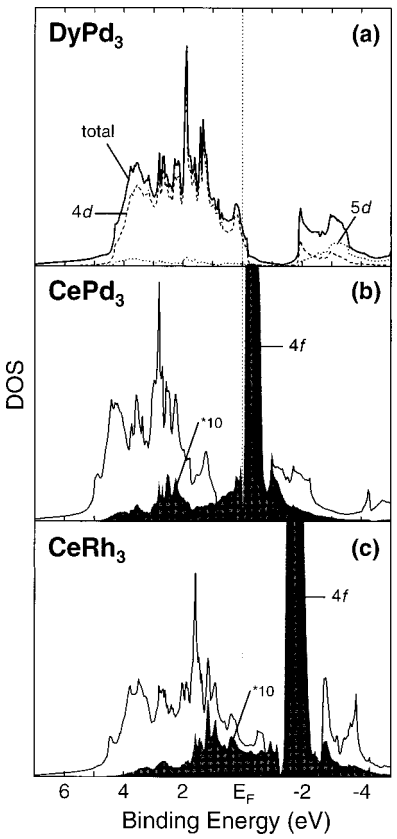

FIG. 6. Calculated total DOS of (a) $DyPd_3$, (b) $CePd_3$, and (c) $CeRh_3$. Partial contributions of Pd $4d$, Dy $5d$, and Ce $4f$ states are shown by broken and dotted lines and shaded areas (with magnification 10), respectively. Since Dy $4f$ states were treated as atomiclike, they are not shown in the DOS.

The more quantitative approach within our optimized LDA-LCAO calculation shows that the predictions of the tight-binding model are basically correct, although the situation is more complex than suggested. Particularly, not only simple charge transfer occurs, but hybrid states between the different RE and TM orbitals are also formed. TM $4d$ and RE $5d$ character is found on both sides of the pseudogap, whereby both states near the top of the valence band and the bottom of the conduction band are dominated by TM $4d$ contributions. This situation is illustrated for $DyPd_3$ in Fig. 6(a). In Ce systems, the situation is not correctly described by a simple depopulation of the Ce $4f$ states, instead hybridization leads to $4f$ admixtures to the valence bands [Fig. 6(b)+6(c)] leaving the total f count almost unchanged.

The main difference between $CePd_3$ and $CeRh_3$ stems from the filling of the ''pure'' $4f$ band, which is characterized by only weak valence-band admixtures giving rise to the prominent $4f$ peak in the calculated DOS. While this band is slightly occupied in $CePd_3$, it becomes empty in $CeRh_3$. Here the whole f count of about 0.8 electrons per formula unit is found in itinerant hybrid states.[11,22]

This fact explains the experimental finding that the BIS spectrum of $CeRh_3$ reveals only a huge $4f^1$ final state, that is close in energy to the calculated position of the Ce $4f$ band, while the BIS spectrum of $CePd_3$ displays both $4f^1$ and $4f^2$ components (Fig. 7). The lack of the $4f^2$ state and the good agreement with the single-particle calculation have been

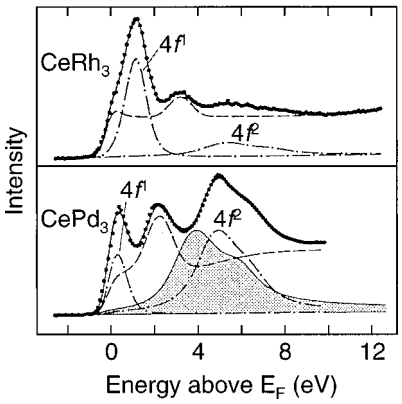

FIG. 7. BIS spectra of $CePd_3$ and $CeRh_3$ as compared to the $4f$ emission of γ-Ce (shaded subspectrum). Subspectra denote the contributions of $4f$ states (dash-dotted) and non-$4f$-derived valence states (dashed) (from Ref. 24).

taken previously as experimental evidence for an itinerant character of the f states in $CeRh_3$. On the basis of the present results, this point should be discussed in more detail. The question of whether electron states should be taken as localized or itinerant may be treated in terms of the LDA bandwidth W and the Coulomb-correlation energy U that describes the energy necessary to transfer an electron from one atom to another. If $U \leqslant W$ the state may be considered as itinerant, while for $U \gg W$ the state can be taken as localized. In the present case of $Ce(TM)_3$ compounds, there are basically two kinds of bands containing f character: the ''pure'' $4f$ band with the width $W_f < 1$eV, and the fd hybrid band with the width $W_{fd} \cong 5$eV (Fig. 6). For Ce, the Coulomb-correlation energy U_f amounts to about 6 eV for atomiclike $4f$ states, while a smaller value U_{fd} for hybrid states is expected due to the larger spacial extend of the wave functions. From these considerations, the hybrid states may be taken as itinerant, while the ''pure'' $4f$ band represents states, that are only supposed to be itinerant within a single-particle approximation and should be treated as localized in a more elaborated approach. In $CeRh_3$ solely hybrid states are populated and, therefore, correlation effects will be weak. Thus, no $4f^2$ component is expected in the BIS spectrum of $CeRh_3$. The remaining question is whether the $4f^1$ final state is expected at the energy position of the ''pure'' $4f$ band predicted by the single-particle calculation, or whether the population of a localized $4f$ state within the BIS process leads to an energy relaxation of the system. Here, one may argue that the large f admixture to the valence states allows a complete final-state screening of the electron-addition state in $CeRh_3$ causing an energy position close to the one predicted by the single-particle band-structure calculation. For $CePd_3$, the situation is different, because the ''pure'' $4f$ band is partly occupied. Addition of an extra electron to this band leads to strong correlation effects that now cannot be compensated by final-state screening. Since the ground state can be described by a linear combination of $4f^0$ and $4f^1$ configurations, the electron-addition state should contain $4f^2$ admixtures as well. As a result, both $4f^1$ and $4f^2$ final states appear in the BIS spectrum in Fig. 7, which is not related anymore to the DOS, but may be described within the Anderson single-impurity model.[6,7]

V. SUMMARY

In summary we have shown, that deposition of Ce and Dy on clean Pd(111) and Rh(111) substrates followed by subsequent annealing leads to a sharp (2×2) overstructure in the LEED patterns indicating the formation of ordered thin-film compounds isomorph to $(RE)(TM)_3(111)$. ARPE data of these *in situ* grown ordered films are in good agreement with optimized LDA-LCAO calculations for the respective bulk compounds. Particularly, an experimentally observed shift to higher BE's of the valence band of the Ce-Pd as compared to the Dy-Pd compound is readily reproduced by the band-structure calculation and attributed to a noninteger occupation of Ce $4f$ states. In $CeRh_3$, the ''pure'' $4f$ band is found to be unoccupied, and the whole $4f$ count of the order of 0.8 electrons per formula unit is spread into the valence band. This fact explains the lack of correlation effects noted previously in the $4f$ PE and BIS spectra of this compound.

ACKNOWLEDGMENTS

This work was supported by the Bundesministerium für Bildung, Wissenschaft, Forschung und Technologie (BMBF), Project No. 05 625 ODA; the Deutsche Forschungsgemeinschaft, Project No. LA 655/3-1, Sonderforschungsbereich 463, TP B4; the Graduiertenkolleg ''Struktur und Korrelationseffekte in Festkörpern.'' Expert help by E. Erler, the staff of BESSY, and the group of H. Freund from the Fritz-Haber-Institut Berlin is gratefully acknowledged.

[1] R. Nagarajan, C. Mazumdar, Z. Hossain, S. K. Dhar, K. V. Gopalakrishnan, L. C. Gupta, C. Godart, B. D. Padalia, and R. Vijayaraghavan, Phys. Rev. Lett. **72**, 274 (1994).
[2] R. J. Cava, Nature (London) **367**, 146 (1994).
[3] R. J. Cava, Nature (London) **367**, 252 (1994).
[4] *Handbook on the Physics and Chemistry of Rare Earths*, 1st ed. (North-Holland, Amsterdam, 1987); for a complete overview the reader is referred to this series.
[5] W. E. Gardner, J. Penfold, T. F. Smith, and I. R. Harris, J. Phys. F **2**, 133 (1972).
[6] O. Gunnarsson and K. Schönhammer, Phys. Rev. B **28**, 4315 (1983).
[7] O. Gunnarsson and K. Schönhammer, Phys. Rev. Lett. **50**, 604 (1983).
[8] The same arguments held also for actinide-TM compounds. For example, the U $5f$ states in UPd_3 behave localized, while they show bandlike behavior in URh_3 and in pure U metal.
[9] D. J. Peterman, J. H. Weaver, and M. Croft, Phys. Rev. B **25**, 5530 (1982).
[10] E. Wuilloud, B. Delley, W. D. Schneider, and Y. Baer, Phys. Rev. Lett. **53**, 202 (1984).
[11] E. Weschke, C. Laubschat, R. Ecker, A. Höhr, M. Domke, G. Kaindl, L. Severin, and B. Johansson, Phys. Rev. Lett. **69**, 1792 (1992).
[12] F. Bertran, T. Gourieux, G. Krill, M. F. Ravet-Krill, M. Alnot, J. J. Eberhardt, and W. Felsch, Phys. Rev. B **46**, 7829 (1992).
[13] J. Boysen *et al.* (unpublished).
[14] L. Hedin and B. I. Lundqvist, J. Phys. C **4**, 2064 (1971).
[15] H. Eschrig, *Optimized LCAO Method* (Springer, Berlin, 1989).
[16] M. Richter and H. Eschrig, Solid State Commun. **72**, 263 (1989).
[17] R. Schumann, M. Richter, L. Steinbeck, and H. Eschrig, Phys. Rev. B **52**, 8801 (1995).
[18] N. V. Smith and L. F. Mattheis, Phys. Rev. B **9**, 1341 (1974).
[19] N. V. Smith, Phys. Rev. B **9**, 1365 (1974).
[20] A. Goldman, G. Rosina, E. Bertel, and F. P. Netzer, Z. Phys. B **73**, 479 (1989).
[21] C. König, Z. Phys. B **50**, 33 (1983).
[22] D. J. Peterman, J. H. Weaver, M. Croft, and D. T. Peterson, Phys. Rev. B **27**, 808 (1983).
[23] C. Laubschat, G. Kaindl, E. V. Sampathkumaran, and W. D. Schneider, Solid State Commun. **49**, 339 (1984).
[24] C. Laubschat, W. Grentz, and G. Kaindl, Phys. Rev. B **36**, 8233 (1987).
[25] E. W. Plummer and W. Eberhard, Adv. Chem. Phys. **49**, 533 (1995).
[26] *Binary Alloy and Phase Diagrams*, 2nd ed., edited by T. B. Massalaki, H. Okamoto, P. Subramariam, and L. Kaprzak (American Society for Metals International, Metal Park, Ohio, 1992), Vol. 3.
[27] A. R. Miedema, P. F. de Chatel, and P. R. de Boer, Physica (Utrecht) **100B**, 1 (1980).
[28] J. F. H. van der Veen and D. E. Eastman, Phys. Rev. Lett. **44**, 189 (1980).
[29] M. S. S. Brooks and B. Johansson, in *Handbook of Magnetic Materials*, edited by K. H. J. Buschow (North-Holland, Amsterdam, 1993), Vol. 7.